

Magnetoelectric coupling in multiferroic $\text{CoFe}_2\text{O}_4/(\text{Ba}_{0.95}\text{Ca}_{0.05})(\text{Ti}_{0.89}\text{Sn}_{0.11})\text{O}_3$ core-shell nanofibers elaborated by co-axial electrospinning method

Youness Hadouch^{1,2,*}, Daoud Mezzane^{1,2}, M'barek Amjoud¹, Valentin Laguta^{3,4}, Khalid Hoummada⁵, Voicu Octavian Dolocan⁵, Mustapha Jouiad², Mohammed Lahcini^{1,6}, Hana Uršič⁷, Nikola Novak⁷, Zdravko Kutnjak⁷, Yaovi Gagou², Igor Lukyanchuk², Mimoun El Marssi².

1. *Laboratory of Innovative Materials, Energy and Sustainable Development (IMED), Cadi-Ayyad University, Faculty of Sciences and Technology, BP 549, Marrakech, Morocco.*
2. *Laboratory of Physics of Condensed Matter (LPMC), University of Picardie Jules Verne, Scientific Pole, 33 rue Saint-Leu, 80039 Amiens Cedex 1, France.*
3. *Institute of Physics AS CR, Cukrovarnicka 10, 162 53 Prague, Czech Republic.*
4. *Institute for Problems of Materials Science, National Ac. of Science, Krjijanovskogo 3, Kyiv 03142, Ukraine.*
5. *Aix-Marseille University - CNRS, IM2NP Faculté des Sciences de Saint-Jérôme case 142, 13397 Marseille, France.*
6. *Mohamed VI Polytechnic University, Lot 660, Hay Moulay Rachid. 43150 Ben Guerir Morocco.*
7. *Jozef Stefan Institute, Jamova Cesta 39, 1000 Ljubljana, Slovenia.*

Abstract:

Multiferroic $\text{CoFe}_2\text{O}_4\text{-Ba}_{0.95}\text{Ca}_{0.05}\text{Ti}_{0.89}\text{Sn}_{0.11}\text{O}_3$ core-shell nanofibers (CFO@BCTSn NFs) were synthesized by a sol-gel co-axial electrospinning technique. The scanning electron microscope and transmission electron microscope were used to check nanofibers' core-shell structure/configuration. X-ray diffraction and a high-resolution transmission electron microscope were used to confirm the spinel structure of CFO and the perovskite structure of BCTSn. The magnetic character of the resultant CFO@BCTSn NFs was determined by SQUID magnetometry. The piezoelectricity was verified using piezo-response force microscopy, which revealed an entirely covered ferroelectric shell outline, in accordance with SEM and TEM observations. The magnetoelectric (ME) coefficient was measured as a function of the applied external DC magnetic field. The maximum ME coefficient obtained for the CFO@BCTSn NFs was $346 \text{ mV cm}^{-1} \text{ Oe}^{-1}$. The high magnetoelectric coupling suggests that CFO@BCTSn NFs could be a promising candidate for magnetic field sensor and magnetoelectric device applications.

Keywords: Core-shell; nanofiber; electrospinning; piezoelectric; multiferroic; magnetoelectric.

Declarations

Conflicts of interest/Competing interests

Not applicable

Availability of data and material

Not applicable

Code availability

Not applicable

Ethics approval

Not applicable

Consent to participate

We confirm that all authors mentioned in the manuscript have participated in, read and approved the manuscript, and have given their consent for the submission and subsequent publication of the manuscript.

Author Contribution

All authors certify that they have participated sufficiently in the work to take public responsibility for the content. Furthermore, each author certifies that this work will not be submitted to other journal or published in any other publication before.

Y. Hadouch: Investigation, Methodology, Data Curation, Writing Original Draft, Validation.

D. Mezzane: Visualization, Methodology, Writing - Review & Editing, Validation, Supervision.

M. Amjoud: Visualization, Writing - Review & Editing, Validation, Supervision.

V. Laguta: Writing - Review & Editing, Visualization, validation,

K. Hoummada: Review & Editing, Visualization, validation,

V. Dolocan: Writing - Review & Editing, Visualization, validation,

M. Jouiad: Review & Editing, Visualization, validation,

M. Lahcini: Review & Editing, Visualization, validation,

H. Uršič: Writing - Review & Editing, Visualization, validation,

N. Novak: Review & Editing, Visualization, validation,

Z. Kutnjak: Writing - Review & Editing, Visualization, validation,

Y. Gagou: Formal analysis, Writing, validation, Supervision.

I. Lukyanchuk: Review & Editing, Visualization, validation,

M. El Marssi: Visualization, Validation, Writing - Review & Editing, Supervision.

Consent for publication

We confirm that all the authors mentioned in the manuscript have agreed to publish this paper.

1. Introduction

Magnetoelectric materials have attracted much attention in recent years [1], [2]. The coupling between the electric and the magnetic ordering, they can convert an electric field into a magnetic field and vice versa via the mechanical interactions between the ferroelectric and ferromagnetic phases [3]. This opens the door to a wide range of technological applications, such as multiple-state memory devices that can be written electrically and read magnetically, electrically controlled microwave phase shifter or voltage-controlled ferromagnetic resonance, magnetically controlled electro-optic or piezoelectric devices and magnetoelectric memory cells [4–8].

There are two types of magnetoelectric materials: (i) single-phase multiferroic in which magnetic and electric fields are intrinsically coupled [9], [10]. However, magnetoelectric couplings in this type of materials are typically very weak [11]. (ii) Multi-phase composites with spatially separated piezoelectric and magnetostrictive phases connected through an interface, where the magnetoelectric coupling is induced indirectly via a strain interaction between piezoelectric and magnetostrictive effects [12–23]. The significant factor in achieving strong ME effects in these composites is to transfer as much strain as possible from one phase of the composite to another [2], [24]. As a result, the area of the interface between ferroelectric and ferromagnetic grains is critical in this type of strain-mediated ME coupling [22], [25–28].

Many approaches and designs have been investigated to create hybrid multiferroic composites, called connectives, including 0–3, 1–3 and 2–2 type connectivity [23], [29]. The most studied type of connectivity is 0-3, also known as particulate composites [29–36]. In this type, the magnetic particles are enclosed by the piezoelectric phase. Specifically, these composites are made by combining the piezoelectric and magnetostrictive phases, resulting in inhomogeneous dispersion of the magnetic phase and agglomeration of these particles due to their attractive nature and surface energy. Agglomeration reduces the interface surface between the two ferroic phases, lowering the ME effect [23]. Based on this, the best way to intimate the contact between the two phases is to create one-dimensional (1D) interfaces at the nanoscale [38], [39]. The coaxial core-shell nanofibers, with a large interfacial surface and high surface-to-volume ratio, are the most commonly recommended for meeting these requirements [25–27], [39]. Several techniques, such as template-assisted approaches, hydrothermal methods, and electrospinning techniques, have been used to create 1D multiferroic nanocomposites [41], [42]. In particular, electrospinning is a feasible and adaptable method for creating multiferroic composite NFs with ultra-long and continuous structures. It has many advantages in practice, such as the ability to

control the size of the nanostructures, the high aspect ratio, and the low cost-efficiency. Additionally, it is possible to easily control the properties of nanofibers using electrospinning parameters like the electric field, solution viscosity, humidity, and annealing temperature [43], [44]. On fundamental level the study of the multiferroic nanofibers presents a particular interest. Exotic polar topological states, like vortex and helix polarization tubes were predicted but not yet confirmed experimentally [45]–[49]. Understanding of coupling of such topological formations with magnetism is on track. In a theoretical study published 13 years ago, Zhang et al. showed that nanofiber composites have orders of magnitude stronger magnetoelectric responses than multiferroic composite thin films of similar compositions [1]. Despite all these benefits, very few studies have reported the fabrication of nanostructured composite fibers using a sol-gel assisted electrospinning technique. Furthermore, a small portion of these studies has focused on the magnetoelectric coupling of electrospun fibers [27], [43], [44]. These examples used cobalt ferrite CoFe_2O_4 (CFO) as a magnetostrictive phase with a large magnetoelastic coefficient (greater than 200 ppm) [52]–[55]. Due to its significant piezoelectric properties, $\text{PbZr}_{0.52}\text{Ti}_{0.48}\text{O}_3$ (PZT) is the ferroelectric material most frequently used in these composites [21], [22], [27], [56]. Unfortunately, Pb-based material is restricted globally because of its negative impact on the environment. Barium titanate BaTiO_3 (BT) and its derivatives are therefore the main candidates for a Pb-free multiferroic composite.

We have recently reported results obtained on $(1-x)\text{Ba}_{0.95}\text{Ca}_{0.05}\text{Ti}_{0.89}\text{Sn}_{0.11}\text{O}_3-x\text{CoFe}_2\text{O}_4$ particulate composites, and the maximum ME coefficient has been found around $0.1 \text{ mV cm}^{-1} \text{ Oe}^{-1}$ at 2.1 kOe for $x=0.3$ [57]. This value, while comparable to similar systems, remains low for such a multiferroic application. As reported in this work, the efficiency of ME coupling in BCTSn-CFO ceramic composites can be significantly improved by varying the sizes and shapes of the grains of the piezoelectric and magnetostrictive phases, as well as the synthesis of core-shell nanostructures.

This paper focuses on (i) the synthesis of magnetoelectric core-shell nanofibers with a CoFe_2O_4 core and a $\text{Ba}_{0.95}\text{Ca}_{0.05}\text{Ti}_{0.89}\text{Sn}_{0.11}\text{O}_3$ shell using the electrospinning method and (ii) the investigation of the structural, morphological, magnetic, ferroelectric and magnetoelectric properties of the CFO@BCTSn NFs.

2. Experimental section

2.1. Material synthesis

CFO@BCTSn nanofibers were prepared by sol-gel process based electrospinning method as follows. For CFO solution, 1 mmol of cobalt nitrate hexahydrate ($\text{Co}(\text{NO}_3)_2 \cdot 6\text{H}_2\text{O}$) and 2 mmol iron nitrite nonahydrate ($\text{Fe}(\text{NO}_3)_3 \cdot 9\text{H}_2\text{O}$) were dissolved into a mixed solution of 2 mL of ethanol and 2 mL of N,N-dimethyl formamide (DMF) and stirred continuously for 3 h. BCTSn precursor solution was synthesized by dissolving a stoichiometric portion of barium acetate $\text{Ba}(\text{CH}_3\text{COO})_2$ and calcium acetate $\text{Ca}(\text{CH}_3\text{COO})_2$ in acetic acid and tin chloride ($\text{SnCl}_2 \cdot 2\text{H}_2\text{O}$) in 2-methoxyethanol separately. The polymer solution was prepared by dissolving poly(vinyl pyrrolidone) (PVP) with a molecular weight of 1 300 000 in ethanol under vigorous stirring for 4 h. The CFO and BCTSn solutions were added to the PVP solution and stirred continuously to form homogenous CFO and BCTSn polymer solutions, with the concentration of PVP controlled around 0.045 and 0.030 g mL^{-1} , respectively. Individual polymer solutions were transferred into glass syringes for electrospinning. The coaxial spinneret and electrospinning setup are depicted in **Fig. 1**. The spinning process was performed at DC voltage with a 12 cm distance between the needle tip and collector. The BCTSn and CFO polymer solutions were pumped at a rate of 0.5 and 0.3 mL h^{-1} , respectively. The as-spun NFs were dried at 80 °C under vacuum for 12 h before being annealed at 700 °C for 4 h in an air atmosphere.

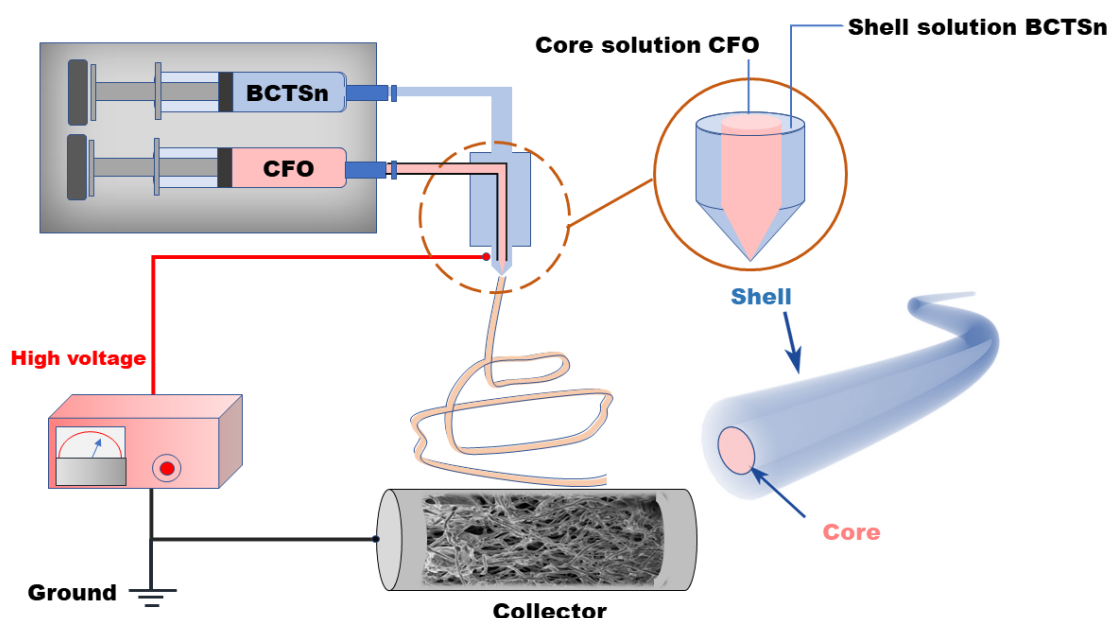


Fig. 1. Coaxial electrospinning of core-shell nanofibers: setup schematics.

2.2. Characterizations

The core-shell nanofibers microstructure was analyzed using scanning electron microscopy (SEM) in a HELIOS 600 nanolab from Thermofisher and a (JEOL – ARM200F Cold FEG) high resolution analytical transmission electron microscope (TEM) operating at 200KV. The XRD patterns of CFO@BCTSn NFs were obtained by X-ray diffraction in the Bragg-Brentano (θ - 2θ) geometry using a Cu $K\alpha$ source ($\lambda K\alpha = 1.54 \text{ \AA}$) at room temperature. The local piezoelectric responses of CFO@BCTSn NFs were investigated by an atomic force microscope (AFM, Jupiter XR Asylum Research, Oxford Instruments, CA, USA) equipped with a piezo-response force module (PFM). Pt-coated silicon tips with a radius of curvature $\sim 10 \text{ nm}$ (OMCL-AC240TM-R3, Olympus, Japan) were used for the PFM analysis. To prevent the CFO@BCTSn NFs from sticking to the PFM tip, the fibers were fixed to the Si substrate by heating at $600 \text{ }^\circ\text{C}$ for 30 min. We chose the nonconductive Si substrate to avoid electrical breakdown through the air and short-circuiting between the tip and the conductive substrate when scanning over the fiber edge and touching the substrate with the PFM tip. Measurements were performed in virtual ground mode as described in our previous work [58], [59]. The images were scanned in dual AC resonance-tracking lateral (DART Lateral) mode. An electrical voltage of 4 V and a frequency of $\sim 690 \text{ kHz}$ was applied. Magnetic properties were measured by demonstrating a magnetic hysteresis (M-H) loop at room temperature using a SQUID magnetometer Quantum Design MPMSXL under a magnetic field range of 0–50 kOe. For magnetoelectric measurements, a conventional Bruker EPR spectrometer EMX plus was used. For this measurement, a rectangular sample with a dimension of $3 \times 5 \times 0.3 \text{ mm}^3$ was prepared by bonding the nanofibers with epoxy resin. Before the measurement, the sample was coated with silver electrodes and poled at room temperature by applying a dc electric field of 10 kV/cm for 10 min (More details are described in Ref. [60]).

3. Results and discussion

3.1 CFO@BCTSn NFs: morphology and structure:

The morphologies of the annealed CFO@BCTSn NFs were observed by SEM and TEM. **Fig. 2a** depicts an SEM image of the CFO@BCTSn NFs, demonstrating that individual NFs have a continuous structure with diameters ranging from 150 to 300 nm. The surface of a single CFO@BCTSn NF is shown in **Fig. 2b**, indicating that the fiber is composed of small grains in the range of tens of nanometers, that may be of the BCTSn phase because they form the fiber's shell. A detailed observations of an individual fiber are depicted in **Figs. 2c and d**. The core and shell are well identified, with a 110 nm diameter CFO core and a 370 nm thick BCTSn shell.

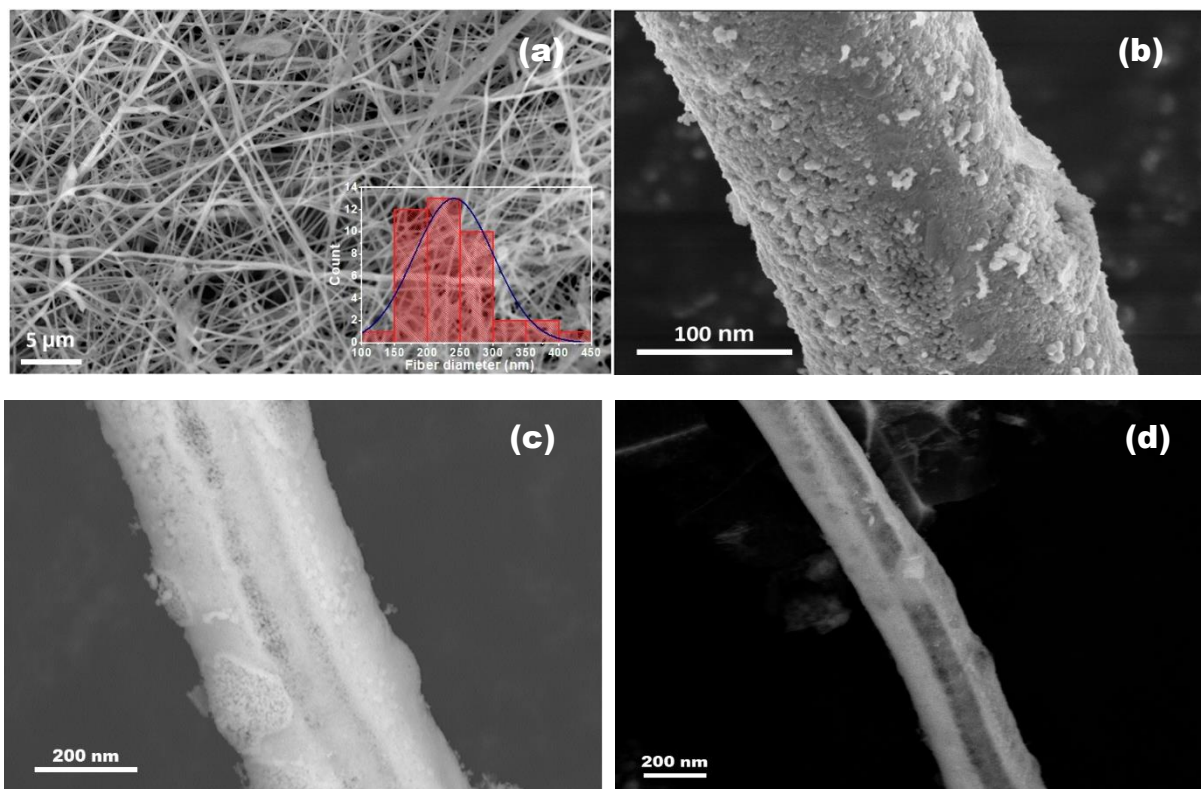


Fig. 2. SEM images of annealed (a) CFO@BCTSn NFs, the inset to the image shows a fiber diameter distribution, (b), (c) and (d) single CFO@BCTSn NF.

The microstructures of the CFO@BCTSn NFs were further investigated by TEM. **Fig. 3a** depicts a TEM image of an individual nanofiber, made up of nanocrystallites of CFO and BCTSn that are connected individually. **Fig. 3b** depicts the interference of two crystallographic orientations originating from BCTSn and CFO crystals. The SAED pattern in the inset of **Fig. 3a** obtained from the red colored-circle zone shows multiple diffraction rings, suggesting a polycrystalline structure of CFO@BCTSn NFs. The crystallographic planes (400), (440), (422) and (620) are assigned to CFO [61], while the planes (220) and (223) are assigned to BCTSn [62], confirming the coexistence of both magnetic and ferroelectric phases.

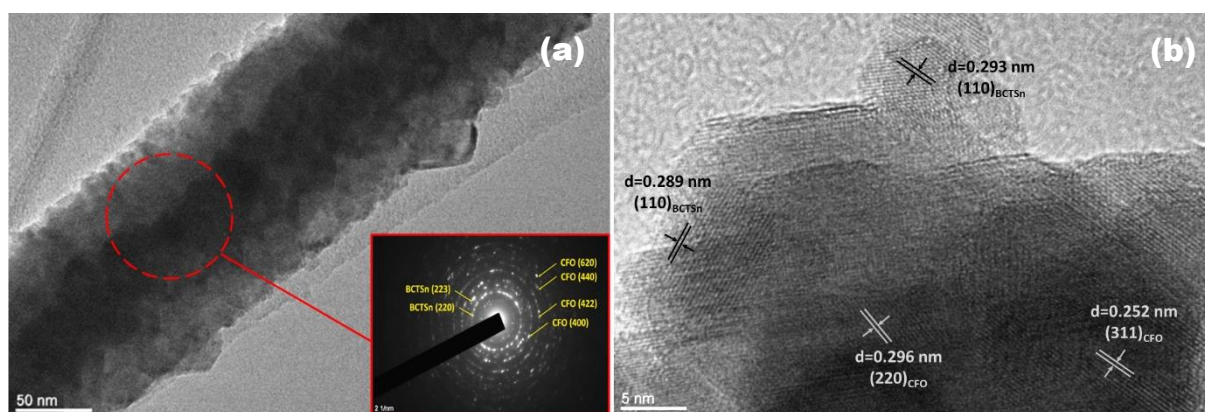


Fig. 3. (a) TEM image of an individual CFO@BCTSn NF, inset in (a): diffraction pattern acquired from the red-colored circle, (b) HRTEM image of CFO@BCTSn NF.

The XRD data of CFO@BCTSn NFs are shown in **Fig. 4a**, which reveals two types of diffraction peaks that are consistent with the Spinel structure's standards (JCPDS No. 01-1121) and the perovskite structure (JCPDS No. 31-0174). Furthermore, the average crystallite size of CFO and BCTSn is estimated to be 4.4 and 5.1 nm, respectively, based on a detailed analysis of the peaks broadening of (311) and (100) reflections using the Debye-Scherrer formula[62].

The lattice strain in the CFO@BCTSn NFs is calculated using the Williamson-Hall (W-H) method [21]. The lattice strain of the composite is calculated by considering the peaks in the XRD patterns that correspond to BCTSn, as shown in **Fig. 4a**.

$$\beta \cos \theta = 4 \varepsilon \sin \theta + \frac{k\lambda}{D} \quad (1)$$

where k ($=0.9$) is the shape factor, λ is the wavelength of X-ray, θ is the peak position in degree, D is the average crystallite size, ε is the lattice strain, and β is the full width at half maxima (FWHM). According to equation (1), the plot of $\beta \cos \theta$ versus $4 \sin \theta$ should be a linear function, with the slope indicating the strain in the sample. The lattice strain in CFO@BCTSn NFs is $3.64 \cdot 10^{-3}$. This positive value indicates that the strain in the CFO@BCTSn NFs is tensile [21]. It is well known that lattice strain improves polarization stability and piezoelectric properties in the ferroelectric phase of magnetoelectric composite materials [63], [64].

These obtained results confirm the successful preparation of the 1D CFO@BCTSn NFs multiferroic composite material. The multiferroic properties of the CFO@BCTSn NFs are then investigated by measuring their ferromagnetic, ferroelectric and ME coupling.

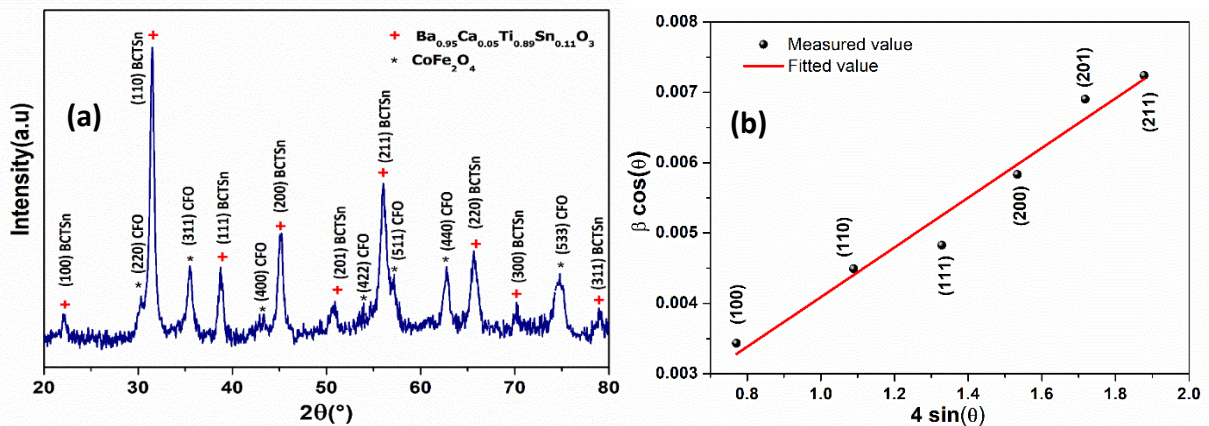


Fig. 4. (a) Room temperature XRD pattern and (b) Williamson-Hall (W-H) plot of CFO@BCTSn NFs.

3.2 CFO@BCTSn NFs magnetic properties:

The magnetization vs. magnetic field for CFO@BCTSn NFs at 300 K is shown in **Fig 5**. The M-H loop shows a classical ferromagnetic behavior with a very small paramagnetic component due to the possible interdiffusion of a small number of magnetic atoms in the shell. The inset displays a zoom of the area depicted by the rectangle. We determine a coercive field of 221 Oe, a remanent magnetization M_r of 1.43 emu g^{-1} (only 12 % of the maximum value) and a maximum magnetization M_s of 11.63 emu g^{-1} at room temperature. It should be stressed that the magnetization is not completely saturated under 25 kOe.

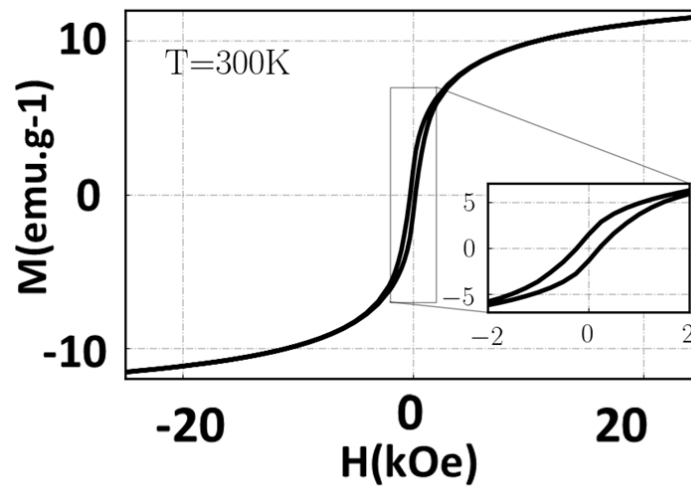


Fig. 5. Magnetic hysteresis loops for the CFO@BCTSn NFs at room temperature.

3.3 Ferroelectric properties of CFO@BCTSn NFs:

The lateral PFM images of the nanofibers on the Si substrate are shown in **Fig. 6**. Comparing the topography panels (a) and (b) with the PFM panels (c) and (d), it is clear where the nanofibers are positioned on the Si substrate. The nanofibers show enhanced piezoelectric response, which can be seen as bright areas in panel (c), except in the center of the nanofibers, where there is no piezoelectric signal (the dark spots). Some examples of areas without piezoelectric signals are marked with blue arrows. These areas most likely correspond to the magnetic phase inside the nanofibers.

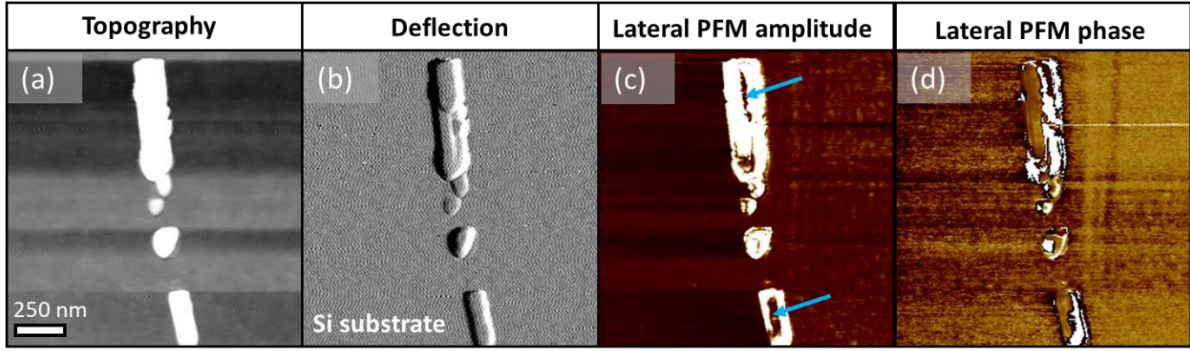


Fig. 6. AFM/PFM images of CFO@BCTS_n NFs: AFM topography (a) height and (b) deflection and lateral PFM (c) amplitude and (d) phase images.

3.4 Magnetolectric properties of CFO@BCTS_n NFs:

The ME coupling coefficient between the BCTS_n and CFO phases was calculated using the following formula described in our previous study [57].

$$\alpha_{ME} = \left(\frac{\partial E}{\partial H} \right) = \frac{V}{d H_{ac}} \quad (2),$$

where V is the induced ME voltage across the sample, d represents the thickness of the sample, and H_{ac} is the applied AC magnetic field.

The room temperature ME coefficient (α_{ME}) of the CFO@BCTS_n NFs has been measured by applying the AC magnetic field of 1.78 Oe at 564 Hz frequency. The ME coefficient shows a non-linear increase with increasing dc magnetic field, reaching a maximum value of 346 mV cm⁻¹ Oe⁻¹ at the DC magnetic field of 10 kOe, as shown in Fig. 7. Because of the mechanical interactions between the ferrite and ferroelectric/piezoelectric perovskite phases throughout the fiber, the magnetic field induces strain in the ferrite phase, which results in stress in the ferroelectric phase. This stress produces a voltage in the shell via the piezoelectric effect [33].

As discussed in our previous paper [57], the area of the interface between ferroelectric and ferromagnetic phases and phase connectivity are crucial in the strain-mediated ME composites. The improved magnetolectric coefficient obtained in the CFO@BCTS_n NFs directly relates to electrospinning process. Indeed, the CFO@BCTS_n NFs produced by electrospinning comprise nanoscale BCTS_n and CFO grains as shown in SEM images (Fig. 2). Such nanoscale grains can make a large interfacial area, favoring mechanical interactions between the piezoelectric and magnetostrictive phases. In addition, our composite fibers also have good phase-connectivity, as observed in the TEM images (Fig. 3). This can ensure complete strain

transfer between the CFO and BCTSn phases, enhancing the magnetoelectric properties of these composites. As a result, the observed α_{ME} is higher than the $\alpha_{ME}=13.3 \text{ mV cm}^{-1} \text{ Oe}^{-1}$ reported for BaTiO₃/CoFe₂O₄ composite fibers [65], $\alpha_{ME}=150.58 \text{ mV cm}^{-1} \text{ Oe}^{-1}$ reported for CFO@BT@PDA/(P(VDF-TrFE)) and $\alpha_{ME}=51 \text{ mV cm}^{-1} \text{ Oe}^{-1}$ reported for CoFe₂O₄ nanorods embedded in BaTiO₃ matrix [50]. However, the obtained α_{ME} value is lower than $2.95 \cdot 10^4 \text{ mV cm}^{-1} \text{ Oe}^{-1}$ reported for CoFe₂O₄-Pb(Zr_{0.52}Ti_{0.48})O₃ core-shell nanofibers [27], which may be attributed to the d_{33} piezoelectric coefficient of Pb(Zr_{0.52}Ti_{0.48})O₃ that is three or four times higher than that of the co-doped BaTiO₃ [51].

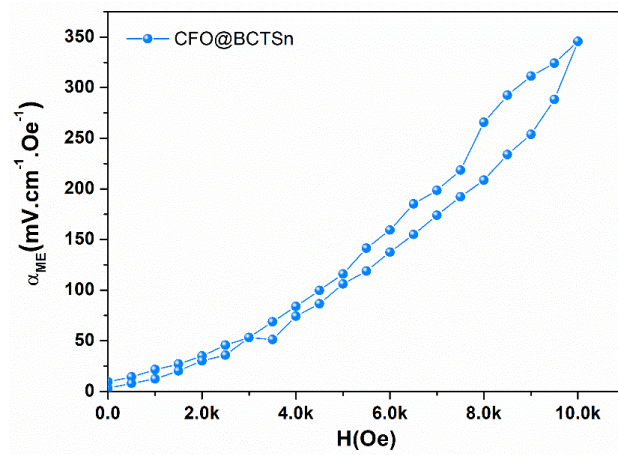


Fig. 7. Dependence of the magnetoelectric coefficient of CFO@BCTSn NFs on the DC magnetic field at room temperature.

4. Conclusion:

In this study, core-shell CoFe₂O₄-Ba_{0.95}Ca_{0.05}Ti_{0.89}Sn_{0.11}O₃ nanofibers were elaborated by the sol-gel electrospinning method. The structural, morphological, and multiferroic properties of these nanofibers were investigated. The presence of perovskite and spinel structures in the CFO@BCTSn NFs was confirmed by XRD and SAED analysis. The morphology of the core-shell nanofibers was observed by SEM and TEM images that endorse the core-shell connectivity. Multiferroic properties of CFO@BCTSn NFs were verified. PFM mappings and M-H hysteresis loops were used to prove that the synthesized fibers had both piezoelectric and ferromagnetic properties. The magnetoelectric coupling coefficient of $346 \text{ mV cm}^{-1} \text{ Oe}^{-1}$, determined experimentally, is significantly higher when compared to the other connectivity types. The high ME coupling was explained by the core-shell fibers' connectivity, which has large interfacial areas and excellent interconnectivity between the two ferroic phases.

Acknowledgements:

This research is financially supported by the European Union Horizon 2020 Research and Innovation actions MSCA-RISE-ENGIMA (No. 778072), MSCA-RISE-MELON (No. 872631). H.U acknowledge the Slovenian Research Agency (N2-0212, P2-0105) and thanks J. Cilenšek and V. Fišinger for help in the laboratory. ZK acknowledge the Slovenian Research Agency support (P1-0125).

References:

- [1] C. L. Zhang, W. Q. Chen, S. H. Xie, J. S. Yang, and J. Y. Li, ‘The magnetoelectric effects in multiferroic composite nanofibers’, *Appl. Phys. Lett.*, vol. 94, no. 10, p. 102907, Mar. 2009, doi: 10.1063/1.3095596.
- [2] A. Baji, Y.-W. Mai, R. Yimmirun, and S. Unruan, ‘Electrospun barium titanate/cobalt ferrite composite fibers with improved magnetoelectric performance’, *RSC Adv.*, vol. 4, no. 98, pp. 55217–55223, 2014, doi: 10.1039/C4RA09449B.
- [3] G. Sreenivasulu, J. Zhang, R. Zhang, M. Popov, V. Petrov, and G. Srinivasan, ‘Multiferroic Core-Shell Nanofibers, Assembly in a Magnetic Field, and Studies on Magneto-Electric Interactions’, *Materials*, vol. 11, no. 1, p. 18, Dec. 2017, doi: 10.3390/ma11010018.
- [4] N. Ortega, A. Kumar, J. F. Scott, and R. S. Katiyar, ‘Multifunctional magnetoelectric materials for device applications’, *J. Phys.: Condens. Matter*, vol. 27, no. 50, p. 504002, Dec. 2015, doi: 10.1088/0953-8984/27/50/504002.
- [5] Y. K. Fetisov and G. Srinivasan, ‘Electric field tuning characteristics of a ferrite-piezoelectric microwave resonator’, *Appl. Phys. Lett.*, vol. 88, no. 14, p. 143503, Apr. 2006, doi: 10.1063/1.2191950.
- [6] W. Eerenstein, N. D. Mathur, and J. F. Scott, ‘Multiferroic and magnetoelectric materials’, *Nature*, vol. 442, no. 7104, pp. 759–765, Aug. 2006, doi: 10.1038/nature05023.
- [7] C.-W. Nan, M. I. Bichurin, S. Dong, D. Viehland, and G. Srinivasan, ‘Multiferroic magnetoelectric composites: Historical perspective, status, and future directions’, *Journal of Applied Physics*, vol. 103, no. 3, p. 031101, Feb. 2008, doi: 10.1063/1.2836410.
- [8] M. Fiebig, ‘Revival of the magnetoelectric effect’, *J. Phys. D: Appl. Phys.*, vol. 38, no. 8, pp. R123–R152, Apr. 2005, doi: 10.1088/0022-3727/38/8/R01.
- [9] H. J. Xiang, S.-H. Wei, M.-H. Whangbo, and J. L. F. Da Silva, ‘Spin-Orbit Coupling and Ion Displacements in Multiferroic TbMnO₃’, *Phys. Rev. Lett.*, vol. 101, no. 3, p. 037209, Jul. 2008, doi: 10.1103/PhysRevLett.101.037209.
- [10] C.-Y. Kuo *et al.*, ‘Single-domain multiferroic BiFeO₃ films’, *Nat Commun*, vol. 7, no. 1, p. 12712, Nov. 2016, doi: 10.1038/ncomms12712.

- [11] P. R. Mickel, H. Jeon, P. Kumar, A. Biswas, and A. F. Hebard, 'Proximate transition temperatures amplify linear magnetoelectric coupling in strain-disordered multiferroic BiMnO₃', *Phys. Rev. B*, vol. 93, no. 13, p. 134205, Apr. 2016, doi: 10.1103/PhysRevB.93.134205.
- [12] C. M. Kanamadi *et al.*, 'Dielectric and magnetic properties of (x)CoFe₂O₄+(1-x) Ba_{0.8}Sr_{0.2}TiO₃ magnetoelectric composites', *Materials Chemistry and Physics*, vol. 116, no. 1, pp. 6–10, Jul. 2009, doi: 10.1016/j.matchemphys.2009.03.003.
- [13] V. V. Shvartsman, F. Alawneh, P. Borisov, D. Kozodaev, and D. C. Lupascu, 'Converse magnetoelectric effect in CoFe₂O₄–BaTiO₃ composites with a core–shell structure', *Smart Mater. Struct.*, vol. 20, no. 7, p. 075006, Jul. 2011, doi: 10.1088/0964-1726/20/7/075006.
- [14] M. G. Majumdar, 'Analysis of Stress-Coupled Magneto-Electric Effect in BaTiO₃-CoFe₂O₄ Composites using Raman Spectroscopy', vol. 3, no. 11, p. 8, 2012.
- [15] R.-F. Zhang, C.-Y. Deng, L. Ren, Z. Li, and J.-P. Zhou, 'Dielectric, ferromagnetic and magnetoelectric properties of BaTiO₃–Ni_{0.7}Zn_{0.3}Fe₂O₄ composite ceramics', *Materials Research Bulletin*, vol. 48, no. 10, pp. 4100–4104, Oct. 2013, doi: 10.1016/j.materresbull.2013.06.026.
- [16] A. S. Kumar, C. S. C. Lekha, S. Vivek, K. Nandakumar, M. R. Anantharaman, and S. S. Nair, 'Effect of CoFe₂O₄ weight fraction on multiferroic and magnetoelectric properties of (1-x)Ba_{0.85}Ca_{0.15}Zr_{0.1}Ti_{0.9}O₃ – xCoFe₂O₄ particulate composites', *J Mater Sci: Mater Electron*, vol. 30, no. 9, pp. 8239–8248, May 2019, doi: 10.1007/s10854-019-01140-3.
- [17] Y. Wang, Y. Pu, Y. Shi, and Y. Cui, 'Ferroelectric, magnetic, magnetoelectric properties of the Ba_{0.9}Ca_{0.1}Ti_{0.9}Zr_{0.1}O₃/CoFe₂O₄ laminated composites', *J Mater Sci: Mater Electron*, vol. 28, no. 15, pp. 11125–11131, Aug. 2017, doi: 10.1007/s10854-017-6899-1.
- [18] D. Patil *et al.*, 'Large Longitudinal Magnetoelectric Coupling in NiFe₂O₄ –BaTiO₃ Laminates', *Appl. Phys. Express*, vol. 4, no. 7, p. 073001, Jun. 2011, doi: 10.1143/APEX.4.073001.
- [19] L. Kola, A. B. Swain, V. Subramanian, and P. Murugavel, 'Large magnetoelectric response in lead free BaTi_{1-x}Sn_xO₃/NiFe₂O₄ bilayer laminated composites', *J Mater Sci: Mater Electron*, vol. 30, no. 7, pp. 6725–6733, Apr. 2019, doi: 10.1007/s10854-019-00984-z.
- [20] L. K. Pradhan, R. Pandey, R. Kumar, and M. Kar, 'Lattice strain induced multiferroicity in PZT-CFO particulate composite', *Journal of Applied Physics*, vol. 123, no. 7, p. 074101, Feb. 2018, doi: 10.1063/1.5008607.
- [21] S. K. Yadav and J. Hemalatha, 'Electrospinning and characterization of magnetoelectric NdFeO₃-PbZr_{0.52}Ti_{0.48}O₃ Core–Shell nanofibers', *Ceramics International*, vol. 48, no. 13, pp. 18415–18424, Jul. 2022, doi: 10.1016/j.ceramint.2022.03.110.
- [22] S. H. Xie, J. Y. Li, Y. Y. Liu, L. N. Lan, G. Jin, and Y. C. Zhou, 'Electrospinning and multiferroic properties of NiFe₂O₄–Pb(Zr_{0.52}Ti_{0.48})O₃ composite nanofibers', *J. Appl. Phys.*
- [23] P. Kaviraj, R. Pramanik, and A. Arockiarajan, 'Influence of individual phases and temperature on properties of CoFe₂O₄-BaTiO₃ magnetoelectric core-shell nanocomposites', *Ceramics International*, vol. 45, no. 9, pp. 12344–12352, Jun. 2019, doi: 10.1016/j.ceramint.2019.03.153.

- [24] W. Huang, S. Yang, and X. Li, 'Multiferroic heterostructures and tunneling junctions', *Journal of Materiomics*, vol. 1, no. 4, pp. 263–284, Dec. 2015, doi: 10.1016/j.jmat.2015.08.002.
- [25] Y. Liu *et al.*, 'Converse magneto-electric effects in a core-shell multiferroic nanofiber by electric field tuning of ferromagnetic resonance', *Sci Rep*, vol. 10, no. 1, p. 20170, Nov. 2020, doi: 10.1038/s41598-020-77041-x.
- [26] A. M. Molavi and P. Alizadeh, 'Electrospinning of multiferroic $\text{CoFe}_2\text{O}_4@ \text{Ba}(\text{Zr}_{0.2}\text{Ti}_{0.8})\text{O}_3-0.5(\text{Ba}_{0.7}\text{Ca}_{0.3})\text{TiO}_3$ nano-structured fibers via two different routes', *Materials Characterization*, vol. 172, p. 110880, Feb. 2021, doi: 10.1016/j.matchar.2021.110880.
- [27] S. Xie, F. Ma, Y. Liu, and J. Li, 'Multiferroic $\text{CoFe}_2\text{O}_4-\text{Pb}(\text{Zr}_{0.52}\text{Ti}_{0.48})\text{O}_3$ core-shell nanofibers and their magnetoelectric coupling', *Nanoscale*, vol. 3, no. 8, p. 3152, 2011, doi: 10.1039/c1nr10288e.
- [28] C.-W. Nan, M. I. Bichurin, S. Dong, D. Viehland, and G. Srinivasan, 'Multiferroic magnetoelectric composites: Historical perspective, status, and future directions', *Journal of Applied Physics*, vol. 103, no. 3, p. 031101, Feb. 2008, doi: 10.1063/1.2836410.
- [29] A. Lyubchik *et al.*, 'Nanocrystalline thin film silicon solar cells: A deeper look into p/i interface formation', *Thin Solid Films*, vol. 591, pp. 25–31, Sep. 2015, doi: 10.1016/j.tsf.2015.08.016.
- [30] D. Padmapriya *et al.*, 'Composition-dependent structural, electrical, magnetic and magnetoelectric properties of $(1-x)\text{BaTiO}_3-x\text{CoFe}_2\text{O}_4$ particulate composites', *Bull Mater Sci*, vol. 43, no. 1, p. 276, Dec. 2020, doi: 10.1007/s12034-020-02243-y.
- [31] J. Rani, K. L. Yadav, and S. Prakash, 'Dielectric and magnetic properties of $x\text{CoFe}_2\text{O}_4-(1-x)[0.5\text{Ba}(\text{Zr}_{0.2}\text{Ti}_{0.8})\text{O}_3-0.5(\text{Ba}_{0.7}\text{Ca}_{0.3})\text{TiO}_3]$ composites', *Materials Research Bulletin*, vol. 60, pp. 367–375, Dec. 2014, doi: 10.1016/j.materresbull.2014.09.013.
- [32] P. Praveen J, V. R. Monaji, S. D. Kumar, V. Subramanian, and D. Das, 'Enhanced magnetoelectric response from lead-free $(\text{Ba}_{0.85}\text{Ca}_{0.15})(\text{Zr}_{0.1}\text{Ti}_{0.9})\text{O}_3-\text{CoFe}_2\text{O}_4$ laminate and particulate composites', *Ceramics International*, vol. 44, no. 4, pp. 4298–4306, Mar. 2018, doi: 10.1016/j.ceramint.2017.12.018.
- [33] A. A. Momin, M. A. Zubair, Md. F. Islam, and A. K. M. A. Hossain, 'Enhance magnetoelectric coupling in $x\text{Li}_{0.1}\text{Ni}_{0.2}\text{Mn}_{0.6}\text{Fe}_{2.1}\text{O}_4-(1-x)\text{BiFeO}_3$ multiferroic composites', *J Mater Sci: Mater Electron*, vol. 30, no. 14, pp. 13033–13046, Jul. 2019, doi: 10.1007/s10854-019-01665-7.
- [34] T. Walther, U. Straube, R. Köferstein, and S. G. Ebbinghaus, 'Hysteretic magnetoelectric behavior of $\text{CoFe}_2\text{O}_4-\text{BaTiO}_3$ composites prepared by reductive sintering and reoxidation', *J. Mater. Chem. C*, vol. 4, no. 21, pp. 4792–4799, 2016, doi: 10.1039/C6TC00995F.
- [35] M. Breitenbach, H. Deniz, and S. G. Ebbinghaus, 'Magnetoelectric and HR-STEM investigations on eutectic $\text{CoFe}_2\text{O}_4-\text{Ba}_{1-x}\text{Sr}_x\text{TiO}_3$ composites', *Journal of Physics and Chemistry of Solids*, vol. 135, p. 109076, Dec. 2019, doi: 10.1016/j.jpccs.2019.109076.
- [36] P. Pan, J. Tao, F. Ma, and N. Zhang, 'Magnetodielectric effect in $(1-x)(\text{Ba}_{0.88}\text{Ca}_{0.12})(\text{Ti}_{0.88}\text{Zr}_{0.12})\text{O}_3-x\text{CoFe}_2\text{O}_4$ ', *Journal of Magnetism and Magnetic Materials*, vol. 453, pp. 91–95, May 2018, doi: 10.1016/j.jmmm.2017.12.107.

- [37]S. Agarwal, O. F. Caltun, and K. Sreenivas, 'Magneto electric effects in BaTiO₃-CoFe₂O₄ bulk composites', *Solid State Communications*, vol. 152, no. 21, pp. 1951–1955, Nov. 2012, doi: 10.1016/j.ssc.2012.08.002.
- [38]Z. Zhang *et al.*, 'Mesoporous Silica-Coated Gold Nanorods as a Light-Mediated Multifunctional Theranostic Platform for Cancer Treatment', *Adv. Mater.*, vol. 24, no. 11, pp. 1418–1423, Mar. 2012, doi: 10.1002/adma.201104714.
- [39]J. F. Scott, 'Applications of magnetoelectrics', *J. Mater. Chem.*, vol. 22, no. 11, p. 4567, 2012, doi: 10.1039/c2jm16137k.
- [40]M. Cernea *et al.*, 'Piezoelectric/ferromagnetic BNT-BT0.08/CoFe₂O₄ coaxial core-shell composite nanotubes for nanoelectronic devices', *Journal of Alloys and Compounds*, vol. 752, pp. 381–388, Jul. 2018, doi: 10.1016/j.jallcom.2018.04.146.
- [41]B. Fu, R. Lu, K. Gao, Y. Yang, and Y. Wang, 'Substrate clamping effect onto magnetoelectric coupling in multiferroic BaTiO₃-CoFe₂O₄ core-shell nanofibers via coaxial electrospinning', *EPL*, vol. 112, no. 2, p. 27002, Oct. 2015, doi: 10.1209/0295-5075/112/27002.
- [42]T. L. Makarova *et al.*, 'Assessing carbon nanotube arrangement in polystyrene matrix by magnetic susceptibility measurements', *Carbon*, vol. 96, pp. 1077–1083, Jan. 2016, doi: 10.1016/j.carbon.2015.10.065.
- [43]Z. Wang *et al.*, 'Preparation of One-Dimensional CoFe₂O₄ Nanostructures and Their Magnetic Properties', *J. Phys. Chem. C*, vol. 112, no. 39, pp. 15171–15175, Oct. 2008, doi: 10.1021/jp802614v.
- [44]J. Fu *et al.*, 'Unique magnetic properties and magnetization reversal process of CoFe₂O₄ nanotubes fabricated by electrospinning', *Nanoscale*, vol. 4, no. 13, p. 3932, 2012, doi: 10.1039/c2nr30487b.
- [45]I. I. Naumov, L. Bellaiche, and H. Fu, 'Unusual phase transitions in ferroelectric nanodisks and nanorods', vol. 432, 2004.
- [46]L. Lahoche, I. Luk'Yanchuk, and G. Pascoli, 'STABILITY OF VORTEX PHASES IN FERROELECTRIC EASY-PLANE NANO-CYLINDERS', *Integrated Ferroelectrics*, vol. 99, no. 1, pp. 60–66, Jun. 2008, doi: 10.1080/10584580802107684.
- [47]S. Prosandeev *et al.*, 'Natural optical activity and its control by electric field in electrotoroidic systems', *Phys. Rev. B*, vol. 87, no. 19, p. 195111, May 2013, doi: 10.1103/PhysRevB.87.195111.
- [48]M. A. Pavlenko *et al.*, 'Phase Diagram of a Strained Ferroelectric Nanowire', *Crystals*, vol. 12, no. 4, p. 453, Mar. 2022, doi: 10.3390/cryst12040453.
- [49]S. Kondovych, M. Pavlenko, Y. Tikhonov, A. Razumnaya, and I. Lukyanchuk, 'Vortex states in a PbTiO₃ ferroelectric cylinder'. arXiv, Oct. 29, 2022. Accessed: Feb. 23, 2023. [Online]. Available: <http://arxiv.org/abs/2112.10129>
- [50]Y. Deng *et al.*, 'Three-dimensional phases-connectivity and strong magnetoelectric response of self-assembled feather-like CoFe₂O₄-BaTiO₃ nanostructures', *Chemical Physics Letters*, vol. 496, no. 4–6, pp. 301–305, Aug. 2010, doi: 10.1016/j.cplett.2010.07.048.

- [51] J. Hao, W. Li, J. Zhai, and H. Chen, 'Progress in high-strain perovskite piezoelectric ceramics', *Materials Science and Engineering: R: Reports*, vol. 135, pp. 1–57, Jan. 2019, doi: 10.1016/j.mser.2018.08.001.
- [52] S. Amiri and H. Shokrollahi, 'The role of cobalt ferrite magnetic nanoparticles in medical science', *Materials Science and Engineering: C*, vol. 33, no. 1, pp. 1–8, Jan. 2013, doi: 10.1016/j.msec.2012.09.003.
- [53] R. Safi, A. Ghasemi, R. Shoja-Razavi, E. Ghasemi, and T. Sodaee, 'Rietveld structure refinement, cations distribution and magnetic features of CoFe_2O_4 nanoparticles synthesized by coprecipitation, hydrothermal, and combustion methods', *Ceramics International*, vol. 42, no. 5, pp. 6375–6382, Apr. 2016, doi: 10.1016/j.ceramint.2016.01.032.
- [54] Q. Lin, J. Lin, Y. He, R. Wang, and J. Dong, 'The Structural and Magnetic Properties of Gadolinium Doped CoFe_2O_4 Nanoferrites', *Journal of Nanomaterials*, vol. 2015, pp. 1–6, 2015, doi: 10.1155/2015/294239.
- [55] Y. Hadouch, 'Enhanced Relative cooling Power and large inverse magnetocaloric effect of cobalt ferrite nanoparticles synthesized by auto-combustion method', *Journal of Magnetism and Magnetic Materials*, p. 8, 2022.
- [56] S. H. Xie *et al.*, 'Multiferroic CoFe_2O_4 - $\text{Pb}(\text{Zr}_{0.52}\text{Ti}_{0.48})\text{O}_3$ nanofibers by electrospinning', *Appl. Phys. Lett.*, vol. 92, no. 6, p. 062901, Feb. 2008, doi: 10.1063/1.2837185.
- [57] Y. Hadouch, 'Piezoelectric, magnetic and magnetoelectric properties of a new lead-free multiferroic $(1-x)\text{Ba}_{0.95}\text{Ca}_{0.05}\text{Ti}_{0.89}\text{Sn}_{0.11}\text{O}_3$ - $(x)\text{CoFe}_2\text{O}_4$ particulate composites', *J Mater Sci*, 2023.
- [58] Z. Hanani *et al.*, 'A flexible self-poled piezocomposite nanogenerator based on $\text{H}_2(\text{Zr}_{0.1}\text{Ti}_{0.9})_3\text{O}_7$ nanowires and polylactic acid biopolymer', *Sustainable Energy Fuels*, vol. 6, no. 8, pp. 1983–1991, 2022, doi: 10.1039/D2SE00234E.
- [59] D. Makovec *et al.*, 'Ferroelectric bismuth-titanate nanoplatelets and nanowires with a new crystal structure', *Nanoscale*, vol. 14, no. 9, pp. 3537–3544, 2022, doi: 10.1039/D2NR00307D.
- [60] V. V. Laguta *et al.*, 'Room-temperature paramagnetoelectric effect in magnetoelectric multiferroics $\text{Pb}(\text{Fe}_{1/2}\text{Nb}_{1/2})\text{O}_3$ and its solid solution with PbTiO_3 ', *J Mater Sci*, vol. 51, no. 11, pp. 5330–5342, Jun. 2016, doi: 10.1007/s10853-016-9836-4.
- [61] Z. Zi, Y. Sun, X. Zhu, Z. Yang, J. Dai, and W. Song, 'Synthesis and magnetic properties of CoFe_2O_4 ferrite nanoparticles', *Journal of Magnetism and Magnetic Materials*, vol. 321, no. 9, pp. 1251–1255, May 2009, doi: 10.1016/j.jmmm.2008.11.004.
- [62] Y. Hadouch *et al.*, 'Electrocaloric effect and high energy storage efficiency in lead-free $\text{Ba}_{0.95}\text{Ca}_{0.05}\text{Ti}_{0.89}\text{Sn}_{0.11}\text{O}_3$ ceramic elaborated by sol-gel method', *J Mater Sci: Mater Electron*, vol. 33, no. 4, pp. 2067–2079, Feb. 2022, doi: 10.1007/s10854-021-07411-2.
- [63] K. C. Verma, M. Singh, R. K. Kotnala, and N. Goyal, 'Magnetic field control of polarization/capacitance/voltage/resistance through lattice strain in BaTiO_3 - CoFe_2O_4 multiferroic

nanocomposite', *Journal of Magnetism and Magnetic Materials*, vol. 469, pp. 483–493, Jan. 2019, doi: 10.1016/j.jmmm.2018.09.020.

[64] J. Lyu, I. Fina, R. Solanas, J. Fontcuberta, and F. Sánchez, 'Tailoring Lattice Strain and Ferroelectric Polarization of Epitaxial BaTiO₃ Thin Films on Si(001)', *Sci Rep*, vol. 8, no. 1, p. 495, Jan. 2018, doi: 10.1038/s41598-017-18842-5.

[65] A. Baji, Y.-W. Mai, R. Yimmirun, and S. Unruan, 'Electrospun barium titanate/cobalt ferrite composite fibers with improved magnetoelectric performance', *RSC Adv.*, vol. 4, no. 98, pp. 55217–55223, 2014, doi: 10.1039/C4RA09449B.